Highlights

- Neural trajectories in the hippocampus exhibited greater variability during a working memory (WM) task compared to those in the entorhinal cortex and amygdala regions.

- The distance of neural trajectories between encoding and retrieval states in the hippocampus was memory-load dependent during a WM task.

- Hippocampal neural trajectories fluctuated between the encoding and retrieval states in a task-dependent manner during both baseline and sharp-wave ripple (SWR) periods.

- Hippocampal neural trajectories shifted from encoding to retrieval states during SWR period.

Hippocampal neural fluctuations between memory encoding and retrieval states during a working memory task in humans

Yusuke Watanabe[a,*], Yuji Ikegaya[b,c,d], Takufumi Yanagisawa[a,e]

[a]*Institute for Advanced Cocreation studies, Osaka University, 2-2 Yamadaoka, Suita, 565-0871, Osaka, Japan*
[b]*Graduate School of Pharmaceutical Sciences, The University of Tokyo, 7-3-1 Hongo, Tokyo, 113-0033, Japan*
[c]*Institute for AI and Beyond, The University of Tokyo, 7-3-1 Hongo, Tokyo, 113-0033, Japan*
[d]*Center for Information and Neural Networks, National Institute of Information and Communications Technology, 1-4 Yamadaoka, Suita City, 565-0871, Osaka, Japan*
[e]*Department of Neurosurgery, Osaka University Graduate School of Medicine, 2-2 Yamadaoka, Osaka, 565-0871, Japan*

Abstract

Working memory (WM) ~~is a vital component in numerous~~ plays a critical role in many cognitive functions, ~~yet the complex~~ but the intricate neural mechanisms that ~~sustain its operation are not fully understood. In particular~~support its operation remain elusive. Specifically, while the hippocampus and sharp-wave ripple complexes (SWRs) ~~—~~ – brief, synchronous neural oscillation observed in the hippocampus ~~— are known –~~ are recognized for their roles in memory consolidation and retrieval, their ~~engagement~~ involvement in WM tasks ~~remains unclear. Our current research posits that the~~ has not yet been defined. Current research suggests that during WM tasks, multiunit activity patterns in the hippocampus ~~exhibit unique dynamism during WM tasks, especially~~ display distinctive dynamics, particularly during SWR periods. ~~Our study involved the analysis of a dataset obtained~~ This study analyzed a dataset derived from intracranial electroencephalogram recordings ~~recorded from~~ made in the medial temporal lobe (MTL) of nine individuals with epilepsy ~~performing~~ during an eight-second Sternberg task. We ~~utilized~~ applied Gaussian-process factor analysis to ~~calculate~~ determine low-dimensional neural representations, or 'trajectories,' within the MTL regions ~~during~~ while performing the WM task. ~~Our results revealed that the neural trajectories showed~~ The results indicate significant variations in the hippocampus~~compared to~~ ' neural trajectories compared to those in the entorhinal cortex and amygdala. ~~Furthermore,~~ Additionally, the distance of the trajectory between the encoding and retrieval phases ~~were memory-load dependent . Crucially~~was dependent on memory load. Importantly, hippocampal trajectories during the retrieval phase ~~fluctuated~~ demonstrated variations between encoding and retrieval stages ~~in a task-type dependent manner; especially showing transitions~~ based on task type, particularly showing shifts from encoding to retrieval states during SWRs. ~~Therefore, these observations not only demonstrate FIXME>the integral role of<FIXMEthe hippocampusin FIXME>executing<FIXMEWM tasks but also FIXME>put forth a compelling hypothesis <FIXMEfor further investigation: the FIXME>operational<FIXME~~These findings underline the hippocampus's essential function in performing WM tasks and propose an intriguing hypothesis for future research: the functional state of the hippocampus ~~shifts~~ transition from encoding to retrieval during SWRs.

Keywords: working memory, memory load, hippocampus, sharp-wave ripples, humans

1. Introduction

Working memory (WM) ~~plays a crucial role in~~ significantly influences everyday life, and ~~its neural underpinnings remain an area of ongoing research. The hippocampus, notably~~ the neural bases of this cognitive process continue to be the subject of intensive research. One key focus of this research is the hippocampus, a structure integral to memory ~~, continues to be a primary focus of this investigation~~ functions [1] [2] [3] [4] [5] [6] [7] [8] [9]. ~~Gaining insights into the role~~ A thorough

*Corresponding author. Tel: +81-6-6879-3652

understanding of the hippocampus's role in working memory is ~~vital to deepening our understanding~~ essential for advancing our knowledge of cognitive processes ~~, [FIXMECHECKME>]potentially fostering the progression of~~ and fostering advancements in cognitive training and interventions[<~~FIXMECHECKME ENDS~~].

Current evidence suggests that a transient, synchronized oscillation, ~~referred to as~~ called sharp-wave ripple (SWR) [10], is ~~linked~~ associated with several cognitive functions~~, such as~~ . These include memory replay [11] [12] [13] [14] [15], memory consolidation [16] [17] [18] [19], memory recall [20] [21] [22], and neural plasticity [23] [24]. This ~~evidence indicates the likelihood that SWR could be a critical component~~ association suggests that SWR may be a crucial part of hippocampal processing ~~, contributing~~ that contributes to working memory performance. However, research ~~investigating~~ on the effects of SWRs on working memory ~~remains sparse~~ is relatively scarce [25], and is ~~largely~~ predominantly limited to rodent models ~~participating~~ engaged in navigation tasks~~where the exact~~ , where the timing of memory acquisition and recall is not ~~explicitly distinguished~~clearly defined.

Recent studies ~~indicate that hippocampal neurons exhibit~~ have found low-dimensional representations in the hippocampal neurons during WM tasks. ~~Notably~~Specifically, the firing patterns of place cells [26] [27] [28] [29] [30], ~~located~~ found in the hippocampus, ~~are observed to be encompassed~~ have been identified within a dynamic, nonlinear three-dimensional hyperbolic ~~geometry in rat [31] . Moreover~~space in rats [31]. Additionally, grid cells in the entorhinal cortex (EC)~~– the dominant~~ , which is the main pathway to the hippocampus [32] [33] [34]~~– displayed toroidal topology during exploration [35] in rat. Unfortunately, these investigations are confined to~~ , exhibited a toroidal geometry during exploration in rats [35]. However, these studies are limited by their focus on spatial navigation tasks in rodents, ~~thus imposing limitations on~~ affecting the temporal resolution of WM tasks [~~FIXMECHECKME>~~]~~like when the animal acquire and recallinformation~~such as the timing of information acquisition and recall[<~~FIXMECHECKME ENDS~~]. The ~~generalizability~~ applicability of these findings to human subjects and beyond navigation tasks ~~remains to be established~~still needs to be confirmed.

~~Given these considerations, the current~~ Considering these aspects, the present study aims to ~~validate~~ investigate the hypothesis that hippocampal neurons ~~exhibit distinctive , FIXME>responsible<FIXMErepresentations~~ display distinctive patterns of activity or 'neural trajectories' in low-dimensional spaces, ~~designated as 'neural trajectory, ' FIXME>responsible to <FIXMEWM tasks, especially within SWR periods. To evaluate this claim, we employed~~ particularly during SWR periods, in response to WM tasks. To test this hypothesis, we used a dataset of patients performing an eight-second Sternberg task ~~with high temporal resolution~~ (1 s for fixation, 2 s for encoding, 3 s for maintenance, and 2 s for retrieval) ~~, while their intracranial electroencephalography signals~~ with high temporal resolution. Intracranial electroencephalography (iEEG) signals within the medial temporal lobe (MTL) were ~~being recorded~~ recorded for these patients [36]. To ~~investigate~~ examine low-dimensional neural trajectories, we ~~employed~~ utilized Gaussian-process factor analysis (GPFA), ~~a method renowned~~ an established method for analyzing neural population dynamics [37].

2. Methods

2.1. Dataset

~~A publicly available dataset [36] was used, which consists~~ The dataset employed in this study was publicly available and consisted of nine epilepsy patients performing a modified Sternberg task [36]. This task ~~involves~~ encompassed four phases: fixation (1s), encoding (2s), maintenance (3s), and retrieval (2s)~~[36]~~. During the encoding phase, participants were ~~exposed to~~ presented with four, six, or eight alphabet letters, ~~referred to~~ defined as the set size. ~~Subsequently, they~~ They [FIXME>]~~had~~ were required to[<FIXME] ~~decide~~ ascertain whether a probe letter ~~presented~~ shown during the retrieval phase ~~was previously displayed~~ had appeared before (the correct choice for the Match IN task) or not (the correct choice for the Mismatch OUT task). ~~iEEG signals were recorded at a sampling rate of~~ Intracranial electroencephalography (iEEG) signals were captured with a 32 kHz ~~, within a frequency range of~~ sampling rate within a 0.5–5,000 Hz frequency range,

using depth electrodes ~~implanted in the~~ in medial temporal lobe (MTL) regions: the anterior head of the left and ~~the~~ right hippocampus (AHL and AHR), the posterior body of the hippocampus (PHL and PHR), the entorhinal cortex (ECL and ECR), and the amygdala (AL and AR), as ~~illustrated~~ depicted in Figure 1A and Table 1. The iEEG signals were subsequently downsampled to ~~a rate of~~ 2 kHz. Correlations ~~among~~ between variables such as set size and correct rate were ~~investigated~~ examined (Figure **??**S1). ~~The timings of multiunit spikes were determined by~~ Multiunit spike timings were determined via a spike sorting algorithm [38] using the Combinato package (`https://github.com/jniediek/combinato`)(Figure 1C).

2.2. *Calculation of neural trajectories using GPFA*

Neural trajectories, also ~~termed~~ referred to as 'factors' (Figure 1D), in the hippocampus, EC, and amygdala ~~(Figure 1D), were computed~~ were determined using GPFA [37] applied to the multiunit activity data for each session~~. GPFA was~~ , performed with the elephant package (`https://elephant.readthedocs.io/en/latest/reference/gpfa.html`). The bin size was set to 50 ms, ~~with no~~ without overlaps. Each factor was z-normalized across all sessions~~. The~~ , and the Euclidean distance from the origin (O) was then ~~calculated~~ computed (Figure 1E).

For each trajectory within a region ~~, for instance, AHL, *geometric medians* (*i.e.*,~~ such as AHL, geometric medians (g_F for fixation, g_E for encoding, g_M for maintenance, and g_R for retrieval phase) were ~~determined by calculating~~ calculated by determining the median coordinates of the trajectory during the four phases (Figure 1D). An optimal ~~dimensionality for GPFA was identified as~~ GPFA dimensionality was found to be three using the elbow method ~~, which was derived by investigating~~ obtained by examining the log-likelihood values through a three-fold cross-validation approach (Figure 2B).

2.3. *Identifying SWR candidates from hippocampal regions*

Potential SWR events within the hippocampus were detected using a widely ~~accepted~~ used method [39]. LFP signals from a region of interest (ROI) ~~, such as~~ like AHL, were re-referenced by ~~subtracting an~~ deducting the averaged signal from locations outside the ROI (~~*e.g.*~~for instance, AHR, PHL, PHR, ECL, ECR, AL, and AR) (see Figure 1A). The re-referenced LFP signals were then filtered with a ripple-band filter (80–140 Hz) to ~~identify SWR candidates(=~~ determine SWR candidates, marked as SWR^+ candidates ~~)~~ (see Figure 1B). SWR detection was ~~conducted~~ carried out using a published tool (`https://github.com/Eden-Kramer-Lab/ripple_detection`) [40], with the bandpass range adjusted to 80–140 Hz for humans [21] [22], ~~different from the original~~ unlike the initial 150–250 Hz range typically applied to rodents.

Control events for SWR^+ candidates, labeled as SWR^- candidates, were ~~identified~~ detected by randomly shuffling the timestamps of SWR^+ candidates across all trials and subjects. The resulting SWR^+/SWR^- candidates were then ~~subjected to visual inspection, as shown in~~ visually inspected (Figure 1).

2.4. *Defining SWRs from putative hippocampal CA1 regions*

SWRs were ~~distinguished~~ differentiated from SWR candidates in putative CA1 regions. ~~Initially, these regions were~~ These regions were initially defined as follows: SWR^+/SWR^- candidates in the hippocampus were projected into a two-dimensional space based on overlapping spike counts per unit ~~employing~~ using a supervised method~~using~~ , UMAP (Uniform Manifold Approximation and Projection) [41] (Figure 4A). Clustering validation was performed by ~~computing~~ calculating the silhouette score [42] from clustered samples (Table 2). Regions in the hippocampus, which scored above 0.6 on average across sessions (75th percentile) (Figure 4B), were ~~characterized~~ identified as putative CA1 regions, ~~identifying~~ resulting in the identification of five electrode positions from five patients (Table 3).

SWR^+/SWR^- candidates in ~~the assumed~~ these predetermined CA1 regions were ~~classified~~ categorized as SWR^+/SWR^-, ~~thus relinquishing~~ and thus they no longer retained their candidate status. The duration and ripple band peak amplitude of SWRs were ~~observed~~ found to follow log-normal distributions (Figure 4C & E). Each time period of SWR was partitioned relative to the time from the SWR center into pre- (at −800 to −300 ms from the SWR center), mid- (at −250 to +250 ms), and post-SWR (at +300 to +800 ms) times.

2.5. *Statistical evaluation*

~~The~~ Both the Brunner–Munzel test and the Kruskal-Wallis test were ~~performed~~ executed using the SciPy package in Python [43]. Correlational analysis was ~~performed~~ conducted by determining the rank of the observed correlation coefficient ~~in~~ within its associated set-size-shuffled surrogate using a ~~custom~~ customized Python script. The bootstrap test was implemented ~~using~~ with an in-house Python script.

3. Results

3.1. *iEEG recording and neural trajectory in MTL regions during a Sternberg task*

~~We leveraged a publicly available dataset for this analysis [36]. This dataset encompasses~~ Our analysis employed a publicly accessible dataset [36], which comprises LFP signals (Figure 1A) from MTL regions (Table 1) ~~during~~ recorded during the execution of a modified Sternberg task~~execution. We identified~~ . We extracted SWR^{+} candidates from LFP signals ~~filtered through~~ that were filtered in the 80–140 Hz ripple band (Figure 1B), originating ~~across~~ in all hippocampal regions (refer to Methods ~~). Correspondingly~~section). Meanwhile, SWR^{-} candidates were defined at ~~identical timestamps but shuffled~~ the same timestamps but distributed across different trials (Figure 1). The dataset ~~included~~ also encompassed multiunit spikes (Figure 1C)~~identified~~ , recognized via a spike sorting algorithm [38]. ~~By employing~~ Employing GPFA [37], ~~and using the~~ we applied this to 50-ms windows of binned multiunit activity ~~with no overlaps , we determined~~ without overlaps to determine the neural trajectories~~(or factors)~~ , or factors, of MTL regions by session and region (Figure 1D). We normalized each factor ~~by~~ per session and region, for instance, session #2 in AHL of subject #1. ~~Subsequently, we~~ We then calculated the Euclidean distance from the origin (O) (Figure 1E).

3.2. *Hippocampal neural trajectory correlation with a Sternberg task*

Figure 2A ~~illustrates the cloud~~ exhibits a distribution of median neural trajectories~~of~~ , comprising 50 trials, within the three main factor spaces. ~~We determined~~ Utilizing the elbow method, we established the optimal embedding dimension for the GPFA model ~~to be three , using the elbow method~~ as three (Figure 2B). The trajectory distance from the origin (O) ~~(~~ represented as $\|g_F\|$, $\|g_E\|$, $\|g_M\|$, and $\|g_R\|$ ~~)~~ in the hippocampus ~~exceeded~~ surpassed the corresponding distances in the EC and amygdala (Figure 2C & D).[1]

Similarly, we computed the distances between the geometric medians of four phases, namely $\|g_F g_E\|$, $\|g_F g_M\|$, $\|g_F g_R\|$, $\|g_E g_M\|$, $\|g_E g_R\|$, and $\|g_M g_R\|$. ~~The results indicated~~ Our findings suggest that the hippocampus ~~displayed~~ showed larger distances between phases than ~~both~~ those in the EC and amygdala. [2]

3.3. ~~*Memory-load-dependent*~~ *Memory-load-dependent neural trajectory distance between encoding and retrieval states in the hippocampus*

~~In terms of~~ Regarding memory load in the ~~Stenberg~~ Sternberg task, we ~~identified~~ observed a negative correlation between the correct rate of trials and ~~set size (~~the set size, which denotes the number of letters to ~~encode)~~ be encoded (Figure 3A).[3] ~~Similarly~~Concomitantly, a positive correlation was ~~observed~~ noted between the response time and set size (Figure 3B).[4]. ~~Furthermore, we found~~

Next, we discovered a positive correlation between set size and the trajectory distance ~~between~~ separating the encoding and retrieval phases ($\log_{10}\|g_E g_R\|$) (Figure 3C).[5]. However, distances between other

[1] Hippocampus: Distance = 1.11 [1.01], median [IQR], n = 195,681 timepoints; EC: Distance = 0.94 [1.10], median [IQR], n = 133,761 timepoints; Amygdala: Distance = 0.78 [0.88], median [IQR], n = 165,281 timepoints.

[2] Hippocampus: Distance = 0.60 [0.70], median [IQR], n = 8,772 combinations; EC: Distance = 0.28 [0.52], median [IQR], n = 5,017 combinations ($p < 0.01$; Brunner–Munzel test); Amygdala: Distance = 0.24 [0.42], median [IQR], n = 7,466 combinations ($p < 0.01$; Brunner–Munzel test).

[3] Correct rate: set size four (0.99 ±0.11, mean ±SD; n = 333 trials) vs. set size six (0.93 ±0.26; n = 278 trials; $p < 0.001$, Brunner–Munzel test with Bonferroni correction) and set size eight (0.87 ±0.34; n = 275 trials; $p < 0.05$; Brunner–Munzel test with Bonferroni correction). ~~Overall~~Generally, $p < 0.001$ for Kruskal–Wallis test; correlation coefficient = - 0.20, $p < 0.001$.

[4] Response time: set size four (1.26 ±0.45 s; n = 333 trials) vs. set size six (1.53 ±0.91 s; n = 278 trials) and set size eight (1.66 ±0.80 s; n = 275 trials). All comparisons $p < 0.001$, Brunner–Munzel test with Bonferroni correction; $p < 0.001$ for Kruskal–Wallis test; correlation coefficient = 0.22, $p < 0.001$

[5] Correlation between set size and $\log_{10}(\|g_E g_R\|)$: correlation coefficient = 0.05, $p < 0.001$. Specific values: $\|g_E g_R\|$ = 0.54 [0.70] for set size four, n = 447; $\|g_E g_R\|$ = 0.58 [0.66] for set size six, n = 381; $\|g_E g_R\|$ = 0.61 [0.63] for set size eight, n = 395.

~~combinations of phases did not display~~ phase combinations did not highlight statistically significant correlations (Figures 3D and **??**).

3.4. *Detection of hippocampal SWR from putative CA1 regions*

~~For precision improvement in~~ To enhance the precision of recording sites and SWR detection, we ~~estimated~~ approximated the electrode placements in the CA1 regions of the hippocampus using ~~distinct~~ distinguished multiunit spike patterns during ~~the~~ SWR events. SWR^+/SWR^- candidates from ~~every~~ each session and hippocampal region were embedded in ~~a~~ two-dimensional space using UMAP (Figure 4A).[6] ~~We used~~ With the silhouette score as a ~~metric for quality of~~ quality metric for clustering (Figure 4B and Table 2)~~.~~ ~~Recording sites with~~, recording sites demonstrating an average silhouette score exceeding 0.6 across all sessions were identified as putative CA1 regions.[7] (Tables 2 and 3). We identified five putative CA1 regions, four of which were not ~~labeled~~ indicated as seizure onset zones (Table 1).

Subsequently, SWR^+/SWR^- candidates within these putative CA1 regions were labeled as SWR^+ and SWR^-, respectively[8] (Table 3). Both SWR^+ and SWR^- ~~exhibited the same duration~~manifested similar durations[9] (Figure 4C) due to their definitions ~~,~~and followed a ~~log-distribution. We observed an augmentation in SWR^+ incidence during~~ log-normal distribution. During the initial 400 ms of the retrieval phase, we noted an increase in SWR^+ incidence[10] (Figure 4D). The peak ripple band amplitude of SWR^+ ~~outpaced~~ surpassed that of SWR^- and followed a log-normal distribution (Figure 4E).[11].

[6] Consider the AHL in session #1 of subject #1 ~~, for illustration purposes~~as a case in point.

[7] The identified regions were ~~:~~ the AHL of subject #1, AHR of subject #3, PHL of subject #4, AHL of subject #6, and AHR of subject #9.

[8] These definitions ~~led to~~ produced equal counts for both categories: SWR^+ (n = 1,170) and SWR^- (n = 1,170).

[9] These definitions ~~led to~~ result in equal durations for both categories: SWR^+ (93.0 [65.4] ms) and SWR^- (93.0 [65.4] ms).

[10] SWR^+ increased against the bootstrap sample; 95th percentile = 0.42 [Hz]; $p < 0.05$.

[11] SWR^+ (3.05 [0.85] SD of baseline, median [IQR]; n = 1,170) vs. SWR^- (2.37 [0.33] SD of baseline, median [IQR]; n = 1,170; $p < 0.001$; Brunner–Munzel test).

3.5. *Transient changes in hippocampal neural trajectory during SWR*

We ~~computed~~ assessed the 'distance' of the trajectory from the origin (O) during SWR events in both ~~the~~ encoding and retrieval phases (Figure 5A). Observing the increase in distance during SWR~~as shown~~, as illustrated in Figure 5A, we ~~differentiated~~ categorized each SWR into three stages: pre-, mid-, and post-SWR. ~~Therefore~~Hence, the distances from O during those SWR ~~periods~~ intervals are identified as $\|\text{pre-eSWR}^+\|$, $\|\text{mid-eSWR}^+\|$ ~~among others.~~ and others.

The magnitude of $\|\text{mid-eSWR}^+\|$[12] ~~was greater than~~ exceeded that of $\|\text{pre-eSWR}^+\|$[13], and $\|\text{mid-rSWR}^+\|$[14] was larger than $\|\text{pre-rSWR}^+\|$ in both the Match IN and Mismatch OUT tasks.[15].

3.6. *Visualization of hippocampal neural trajectory during SWR in two-dimensional spaces*

~~Following our observations of~~ Having observed neural trajectory 'jumping' during SWR (Figure 5), we visualized the three-dimensional trajectories of pre-, mid-, and post-SWR events during the encoding and retrieval phases (Figure 6)~~, the distance between which~~. The distance between these was found to be memory-load dependent (Figure 3).

To provide two-dimensional visualization, we linearly aligned peri-SWR trajectories by ~~assigning~~ setting g_E at the origin (0, 0) and g_R at ($\|g_E g_R\|$, 0). ~~Post this~~Subsequently, we rotated these aligned trajectories around the $g_E g_R$ axis (the x axis)~~. Thus,~~ , ensuring that the distances from the origin in the original three-dimensional spaces and angles from $\overrightarrow{g_E g_R}$ are ~~preserved~~ retained in the two-dimensional equivalent.

The scatter plot within these two-dimensional spaces ~~reveals characteristic~~ revealed defining distributions of peri-SWR trajectories based on phases and task types. ~~For instance,~~ A particular example of this is visible in[~~FIXME~~CHEKME>] one can observe[<~~FIXME~~CHEKME] that the magnitude of

[12] 1.25 [1.30], median [IQR], n = 1,281 ~~,~~in the Match IN task; 1.12 [1.35], median [IQR], n = 1,163 ~~,~~in the Mismatch OUT task

[13] 1.08 [1.07], median [IQR], n = 1,149 ~~,~~in the Match IN task; 0.90 [1.12], median [IQR], n = 1,088 ~~,~~in the Mismatch OUT task

[14] 1.32 [1.24], median [IQR], n = 935 ~~,~~in the Match IN task; 1.15 [1.26], median [IQR], n = 891 ~~,~~in the Mismatch OUT task

[15] 1.19 [0.96], median [IQR], n = 673 ~~,~~in the Match IN task; 0.94 [0.88], median [IQR], n = 664 ~~,~~in the Mismatch OUT task

$\|$mid-eSWR$^+\|$ surpasses that of $\|$pre-eSWR$^+\|$ (Figure 6B), which is consistent with our ~~earlier findings~~ previous observations (Figure 5).

3.7. Fluctuations of hippocampal neural trajectories between encoding and retrieval states

~~Next~~Subsequently, we examined trajectory 'direction' in relation to $\overrightarrow{g_E g_R}$. The directions of SWRs were defined by the neural trajectory at −250 ms and +250 ms from their center, *i.e.*, $\overrightarrow{\text{eSWR}^+}$. We calculated the ~~consine~~ cosine similarities between $\overrightarrow{g_E g_R}$, $\overrightarrow{\text{eSWR}}$, and $\overrightarrow{\text{rSWR}}$ in both SWR (SWR$^+$)*andbaselineperiods*(SWR^-)(*Figure* 7*A* − −*D*). $\overrightarrow{\text{rSWR}^-} \cdot \overrightarrow{g_E g_R}$ ~~displayed~~ exhibited a biphasic distribution. ~~By taking~~ By computing the difference between the distribution of $\overrightarrow{\text{rSWR}^+} \cdot \overrightarrow{g_E g_R}$ (Figure 7A & B) and that of $\overrightarrow{\text{rSWR}^-} \cdot \overrightarrow{g_E g_R}$ (Figure 7C & D), we were able to determine the contributions of SWR (Figure 7E & F)~~were calculated, which revealed~~, which indicated a shift in the direction of $\overrightarrow{g_E g_R}$ (Figure 7E & F: *red rectangles*). ~~Moreover~~

Furthermore, $\overrightarrow{\text{eSWR}^+} \cdot \overrightarrow{\text{rSWR}^+}$ was less than $\overrightarrow{\text{eSWR}^-} \cdot \overrightarrow{\text{rSWR}^-}$ ~~solely in~~ strictly in the Mismatch OUT task (Figure 7F: *pink circles*). In ~~simpler terms~~other words, eSWR and rSWR pointed in the opposite direction ~~only in~~ exclusively in the Mismatch OUT task but not ~~in~~ the Match IN task (Figure 7E: *pink circles*).

4. Discussion

5. Discussion

This study ~~hypothesized that within~~ hypothesizes that in low-dimensional spaces during a ~~WM~~ working memory (WM) task in humans, hippocampal neurons form unique trajectories, ~~particularly during SWR~~ primarily during sharp wave-ripple (SWR) periods. Initially, ~~the~~ multiunit spikes in ~~MTL~~ the medial temporal lobe (MTL) regions were projected onto three-dimensional spaces during a Sternberg task using ~~GPFA~~ Gaussian-process factor analysis (GPFA) (Figure 1~~D–E~~ D — E and Figure 2A). The ~~distance of the trajectory~~ trajectory distance across WM phases ($\|g_F g_E\|$, $\|g_F g_M\|$, $\|g_F g_R\|$, $\|g_E g_M\|$, $\|g_E g_R\|$, and $\|g_M g_R\|$) was ~~notably~~ significantly larger in the hippocampus ~~than in the EC~~ compared to the entorhinal cortex (EC) and amygdala (Figure 2E), indicating dynamic neural activity in the hippocampus during the WM task. ~~Further~~Also, in the hippocampus, the trajectory distance between the encoding and retrieval phases ($\|g_F g_E\|$) ~~exhibited a positive correlation~~ correlated positively with memory load (Figure 3~~C–D~~C — D), reflecting WM processing. The hippocampal neural trajectory ~~was found to diverse transiently~~ transiently expanded during SWRs (Figure 5). ~~Finally~~Lastly, the hippocampal neural trajectory ~~switched~~ alternated between encoding and retrieval states, ~~moving~~ transitioning from encoding to retrieval during SWR events (Figure 7). These findings ~~not only explain facets~~ explain aspects of hippocampal neural activity during a WM task in humans ~~but also~~ and offer [FIXME>]new insights into SWRs as a state-switching ~~observation~~ element in hippocampal neural states[<FIXME].

~~We found that the~~ The distance of the neural trajectory across the phases was ~~greater~~ significantly longer in the hippocampus compared to ~~that in~~ the EC and amygdala, ~~even~~ when considering the distance from O in these regions (Figure 2~~C–E~~C — E). This ~~supports~~ establishes the involvement of the hippocampus in the WM task, ~~aligning with previous reports of~~ corroborating previous studies indicating hippocampal persistent firing during the maintenance phase [3] [4] [5] [6]. However, ~~when we applied~~ applying GPFA to multiunit activity during a ~~1-second~~ one-second level resolution of the WM task ~~, we observed~~ revealed that the neural trajectory in low-dimensional space ~~showed~~ presented a memory-load dependency between the encoding and retrieval phases, ~~symbolized~~ denoted as $\|g_E g_R\|$ (Figure 3). These findings ~~corroborate~~ support the association of the hippocampus with WM processing.

Our analysis ~~was confined to putative CA1~~ focused on putative Cornu Ammonis (CA)1 regions (Figure 4), ~~which was bolstered~~ reinforced by several factors. This specific focus ~~stems~~ results from established observations that SWRs synchronize with ~~spike bursts of interneurons and pyramidal neurons~~ interneuron and pyramidal neuron spike bursts [44] [45] [46] [47], potentially within a 50 μm radius of the recording site [48]. ~~We further~~ Furthermore, we identified an increased incidence of SWRs during the first 0–400 ms of the retrieval phase (Figure 4D). This finding ~~harmonizes~~ aligns with

previous reports of heightened SWR occurrence preceding spontaneous verbal recall [21] [22], supporting our results under a triggered retrieval condition. The observed log-normal distributions of both SWR duration and ripple band peak amplitude in this study (Figure 4C & E) ~~is in accordance with the~~ coincide with the current consensus in this field [39]. ~~As a result~~Consequently, our decision to ~~restrict~~ limit recording sites to putative CA1 regions likely contributed to ~~enhancing~~ improving the precision, or true positive rate, of SWR detection. ~~However, the increase in trajectory distance~~ Although, the trajectory distance increase from O during SWRs (Figure 5) might ~~have been skewed~~ be artificially inflated towards higher values due to channel selection~~. However~~, this potential bias does not substantially challenge our ~~primary~~ main findings.

Interestingly, during the retrieval phase, ~~the trajectory directions oscillated~~ trajectory directions alternated between encoding and retrieval states during both baseline and SWR periods in a task-dependent manner (Figure 7C & D). ~~Moreover~~Additionally, the balance of this oscillation ~~shifted~~ transitioned from encoding to retrieval state during SWR events (Figure 7 E & F). These results ~~are consistent with previous reports~~ align with previous studies on the role of SWR in memory retrieval [21] [22]. Our findings ~~highlight a new understanding, suggesting~~ introduce a novel understanding indicating that SWRs occur when the hippocampal representation transitions from encoding to retrieval states. Therefore, these results reveal novel aspects of hippocampal representations, including (i) neuronal oscillation between encoding and retrieval states during a WM task and (ii) SWR serving as a transition trigger for changing neural states.

~~Furthermore~~Moreover, our study ~~uncovered~~ noted differences specific to the WM-task ~~type-specific differences~~ type between encoding- and retrieval-SWRs (Figure 7E–F). Notably, opposing movements of encoding-SWR (eSWR) and retrieval-SWR (rSWR) were not observed in the Match IN task but were apparent in the Mismatch OUT task. ~~These observations can be explained by the memory~~ Memory engram theory [49] ~~. Particularly,~~ might explain these observations: the Match In task ~~provided~~ presented participants with previously ~~presented letters, contrastingly,~~ shown letters, while the Mismatch OUT task introduced a new letter ~~not present~~ absent in the encoding phase. ~~These interpretations underscore~~ This explanation underscores the significant role of SWR in human cognitive processes.

In conclusion, ~~the present investigation demonstrated that~~ this study demonstrates that during a WM task, hippocampal activity oscillates between encoding and retrieval states ~~during a WM task and uniquely transitions~~ and transitions uniquely from encoding to retrieval during SWR ~~incidents~~events. These findings provide ~~meaningful insight~~ significant insights into the neural ~~counterparts~~ correlates and functionality of working memory in the hippocampus.

References

[1] W. B. Scoville, B. Milner, LOSS OF RECENT MEMORY AFTER BILATERAL HIPPOCAMPAL LESIONS, Journal of Neurology, Neurosurgery, and Psychiatry 20 (1) (1957) 11–21. URL https://www.ncbi.nlm.nih.gov/pmc/articles/PMC497229/

[2] L. R. Squire, The Legacy of Patient H.M. for Neuroscience, Neuron 61 (1) (2009) 6–9. doi:10.1016/j.neuron.2008.12.023.
URL https://www.ncbi.nlm.nih.gov/pmc/articles/PMC2649674/

[3] E. Boran, T. Fedele, P. Klaver, P. Hilfiker, L. Stieglitz, T. Grunwald, J. Sarnthein, Persistent hippocampal neural firing and hippocampal-cortical coupling predict verbal working memory load, Science Advances 5 (3) (2019) eaav3687. doi:10.1126/sciadv.aav3687.
URL https://www.science.org/doi/10.1126/sciadv.aav3687

[4] J. Kamiński, S. Sullivan, J. M. Chung, I. B. Ross, A. N. Mamelak, U. Rutishauser, Persistently active neurons in human medial frontal and medial temporal lobe support working memory, Nature Neuroscience 20 (4) (2017) 590–601, number: 4 Publisher: Nature Publishing Group. doi:10.1038/nn.4509.
URL https://www.nature.com/articles/nn.4509

[5] S. Kornblith, R. Q. Quiroga, C. Koch, I. Fried, F. Mormann, Persistent Single-Neuron Activity during Working Memory in the Human Medial Temporal Lobe, Current Biology 27 (7) (2017) 1026–1032, publisher: Elsevier. doi:10.1016/j.cub.2017.02.013.
URL https://www.cell.com/current-biology/abstract/S0960-9822(17)30149-5

[6] M. C. M. Faraut, A. A. Carlson, S. Sullivan, O. Tudusciuc, I. Ross, C. M. Reed, J. M. Chung, A. N. Mamelak, U. Rutishauser, Dataset of human medial temporal lobe single neuron activity during declarative memory encoding and recognition, Scientific Data 5 (1) (2018) 180010, number: 1 Publisher: Nature Publishing Group. doi:10.1038/sdata.2018.10.
URL https://www.nature.com/articles/sdata201810

[7] A. A. Borders, C. Ranganath, A. P. Yonelinas, The hippocampus supports high-precision binding in visual working memory,

Hippocampus 32 (3) (2022) 217–230. doi:10.1002/hipo.23401.

[8] J. Li, D. Cao, S. Yu, X. Xiao, L. Imbach, L. Stieglitz, J. Sarnthein, T. Jiang, Functional specialization and interaction in the amygdala-hippocampus circuit during working memory processing, Nature Communications 14 (1) (2023) 2921, number: 1 Publisher: Nature Publishing Group. doi:10.1038/s41467-023-38571-w.
URL https://www.nature.com/articles/s41467-023-38571-w

[9] V. Dimakopoulos, P. Mégevand, L. H. Stieglitz, L. Imbach, J. Sarnthein, Information flows from hippocampus to auditory cortex during replay of verbal working memory items, eLife 11 (2022) e78677, publisher: eLife Sciences Publications, Ltd. doi:10.7554/eLife.78677.
URL https://doi.org/10.7554/eLife.78677

[10] G. Buzsáki, Hippocampal sharp wave-ripple: A cognitive biomarker for episodic memory and planning, Hippocampus 25 (10) (2015) 1073–1188, _eprint: https://onlinelibrary.wiley.com/doi/pdf/10.1002/hipo.22488. doi:https://doi.org/10.1002/hipo.22488.
URL https://onlinelibrary.wiley.com/doi/abs/10.1002/hipo.22488

[11] M. A. Wilson, B. L. McNaughton, Reactivation of hippocampal ensemble memories during sleep, Science (New York, N.Y.) 265 (5172) (1994) 676–679. doi:10.1126/science.8036517.

[12] Z. Nádasdy, H. Hirase, A. Czurkó, J. Csicsvari, G. Buzsáki, Replay and Time Compression of Recurring Spike Sequences in the Hippocampus, Journal of Neuroscience 19 (21) (1999) 9497–9507, publisher: Society for Neuroscience Section: ARTICLE. doi:10.1523/JNEUROSCI.19-21-09497.1999.
URL https://www.jneurosci.org/content/19/21/9497

[13] A. K. Lee, M. A. Wilson, Memory of sequential experience in the hippocampus during slow wave sleep, Neuron 36 (6) (2002) 1183–1194. doi:10.1016/s0896-6273(02)01096-6.

[14] K. Diba, G. Buzsáki, Forward and reverse hippocampal place-cell sequences during ripples, Nature Neuroscience 10 (10) (2007) 1241–1242, number: 10 Publisher: Nature Publishing Group. doi:10.1038/nn1961.
URL https://www.nature.com/articles/nn1961

[15] T. J. Davidson, F. Kloosterman, M. A. Wilson, Hippocampal replay of extended experience, Neuron 63 (4) (2009) 497–507. doi:10.1016/j.neuron.2009.07.027.

[16] G. Girardeau, K. Benchenane, S. I. Wiener, G. Buzsáki, M. B. Zugaro, Selective suppression of hippocampal ripples impairs spatial memory, Nature Neuroscience 12 (10) (2009) 1222–1223. doi:10.1038/nn.2384.
URL http://www.nature.com/articles/nn.2384

[17] V. Ego-Stengel, M. A. Wilson, Disruption of ripple-associated hippocampal activity during rest impairs spatial learning in the rat, Hippocampus 20 (1) (2010) 1–10. doi:10.1002/hipo.20707.

[18] A. Fernández-Ruiz, A. Oliva, E. Fermino de Oliveira, F. Rocha-Almeida, D. Tingley, G. Buzsáki, Long-duration hippocampal sharp wave ripples improve memory, Science (New York, N.Y.) 364 (6445) (2019) 1082–1086. doi:10.1126/science.aax0758.
URL https://www.ncbi.nlm.nih.gov/pmc/articles/PMC6693581/

[19] J. Kim, A. Joshi, L. Frank, K. Ganguly, Cortical–hippocampal coupling during manifold exploration in motor cortex, Nature (2022) 1–8Publisher: Nature Publishing Group. doi:10.1038/s41586-022-05533-z.
URL https://www.nature.com/articles/s41586-022-05533-z

[20] C.-T. Wu, D. Haggerty, C. Kemere, D. Ji, Hippocampal awake replay in fear memory retrieval, Nature Neuroscience 20 (4) (2017) 571–580. doi:10.1038/nn.4507.

[21] Y. Norman, E. M. Yeagle, S. Khuvis, M. Harel, A. D. Mehta, R. Malach, Hippocampal sharp-wave ripples linked to visual episodic recollection in humans, Science 365 (6454) (2019) eaax1030. doi:10.1126/science.aax1030.
URL https://www.sciencemag.org/lookup/doi/10.1126/science.aax1030

[22] Y. Norman, O. Raccah, S. Liu, J. Parvizi, R. Malach, Hippocampal ripples and their coordinated dialogue with the default mode network during recent and remote recollection, Neuron 109 (17) (2021) 2767–2780.e5, publisher: Elsevier. doi:10.1016/j.neuron.2021.06.020.
URL https://www.cell.com/neuron/abstract/S0896-6273(21)00461-X

[23] C. J. Behrens, L. P. van den Boom, L. de Hoz, A. Friedman, U. Heinemann, Induction of sharp wave–ripple complexes in vitro and reorganization of hippocampal networks, Nature Neuroscience 8 (11) (2005) 1560–1567, number: 11 Publisher: Nature Publishing Group. doi:10.1038/nn1571.
URL https://www.nature.com/articles/nn1571

[24] H. Norimoto, K. Makino, M. Gao, Y. Shikano, K. Okamoto, T. Ishikawa, T. Sasaki, H. Hioki, S. Fujisawa, Y. Ikegaya, Hippocampal ripples down-regulate synapses, Science (New York, N.Y.) 359 (6383) (2018) 1524–1527. doi:10.1126/science.aao0702.

[25] S. P. Jadhav, C. Kemere, P. W. German, L. M. Frank, Awake Hippocampal Sharp-Wave Ripples Support Spatial Memory, Science 336 (6087) (2012) 1454–1458, publisher: American Association for the Advancement of Science. doi:10.1126/science.1217230.
URL https://www.science.org/doi/abs/10.1126/science.1217230

[26] J. O'Keefe, J. Dostrovsky, The hippocampus as a spatial map: Preliminary evidence from unit activity in the freely-moving rat, Brain Research 34 (1971) 171–175, place: Netherlands Publisher: Elsevier Science. doi:10.1016/0006-8993(71)90358-1.

[27] J. O'Keefe, Place units in the hippocampus of the freely moving rat, Experimental Neurology 51 (1) (1976) 78–109. doi:10.1016/0014-4886(76)90055-8.
URL https://www.sciencedirect.com/science/article/pii/0014488676900558

[28] A. D. Ekstrom, M. J. Kahana, J. B. Caplan, T. A. Fields, E. A. Isham, E. L. Newman, I. Fried, Cellular networks underlying human spatial navigation, Nature 425 (6954) (2003) 184–188, number: 6954 Publisher: Nature Publishing Group. doi:10.1038/nature01964.
URL https://www.nature.com/articles/nature01964

[29] K. B. Kjelstrup, T. Solstad, V. H. Brun, T. Hafting, S. Leutgeb,

M. P. Witter, E. I. Moser, M.-B. Moser, Finite Scale of Spatial Representation in the Hippocampus, Science 321 (5885) (2008) 140–143, publisher: American Association for the Advancement of Science. doi:10.1126/science.1157086.
URL https://www.science.org/doi/abs/10.1126/science.1157086

[30] C. D. Harvey, F. Collman, D. A. Dombeck, D. W. Tank, Intracellular dynamics of hippocampal place cells during virtual navigation, Nature 461 (7266) (2009) 941–946, number: 7266 Publisher: Nature Publishing Group. doi:10.1038/nature08499.
URL https://www.nature.com/articles/nature08499

[31] H. Zhang, P. D. Rich, A. K. Lee, T. O. Sharpee, Hippocampal spatial representations exhibit a hyperbolic geometry that expands with experience, Nature Neuroscience (Dec. 2022). doi:10.1038/s41593-022-01212-4.
URL https://www.nature.com/articles/s41593-022-01212-4

[32] P. A. Naber, F. H. Lopes da Silva, M. P. Witter, Reciprocal connections between the entorhinal cortex and hippocampal fields CA1 and the subiculum are in register with the projections from CA1 to the subiculum, Hippocampus 11 (2) (2001) 99–104, _eprint: https://onlinelibrary.wiley.com/doi/pdf/10.1002/hipo.1028. doi:10.1002/hipo.1028.
URL https://onlinelibrary.wiley.com/doi/abs/10.1002/hipo.1028

[33] N. M. van Strien, N. L. M. Cappaert, M. P. Witter, The anatomy of memory: an interactive overview of the parahippocampal–hippocampal network, Nature Reviews Neuroscience 10 (4) (2009) 272–282, number: 4 Publisher: Nature Publishing Group. doi:10.1038/nrn2614.
URL https://www.nature.com/articles/nrn2614

[34] B. A. Strange, M. P. Witter, E. S. Lein, E. I. Moser, Functional organization of the hippocampal longitudinal axis, Nature Reviews Neuroscience 15 (10) (2014) 655–669, number: 10 Publisher: Nature Publishing Group. doi:10.1038/nrn3785.
URL https://www.nature.com/articles/nrn3785

[35] R. J. Gardner, E. Hermansen, M. Pachitariu, Y. Burak, N. A. Baas, B. A. Dunn, M.-B. Moser, E. I. Moser, Toroidal topology of population activity in grid cells, Nature 602 (7895) (2022) 123–128, number: 7895 Publisher: Nature Publishing Group. doi:10.1038/s41586-021-04268-7.
URL https://www.nature.com/articles/s41586-021-04268-7

[36] E. Boran, T. Fedele, A. Steiner, P. Hilfiker, L. Stieglitz, T. Grunwald, J. Sarnthein, Dataset of human medial temporal lobe neurons, scalp and intracranial EEG during a verbal working memory task, Scientific Data 7 (1) (2020) 30, number: 1 Publisher: Nature Publishing Group. doi:10.1038/s41597-020-0364-3.
URL https://www.nature.com/articles/s41597-020-0364-3

[37] B. M. Yu, J. P. Cunningham, G. Santhanam, S. I. Ryu, K. V. Shenoy, M. Sahani, Gaussian-Process Factor Analysis for Low-Dimensional Single-Trial Analysis of Neural Population Activity, Journal of Neurophysiology 102 (1) (2009) 614–635. doi:10.1152/jn.90941.2008.
URL https://www.ncbi.nlm.nih.gov/pmc/articles/PMC2712272/

[38] J. Niediek, J. Boström, C. E. Elger, F. Mormann, Reliable Analysis of Single-Unit Recordings from the Human Brain under Noisy Conditions: Tracking Neurons over Hours, PLOS ONE 11 (12) (2016) e0166598, publisher: Public Library of Science. doi:10.1371/journal.pone.0166598.
URL https://journals.plos.org/plosone/article?id=10.1371/journal.pone.0166598

[39] A. A. Liu, S. Henin, S. Abbaspoor, A. Bragin, E. A. Buffalo, J. S. Farrell, D. J. Foster, L. M. Frank, T. Gedankien, J. Gotman, J. A. Guidera, K. L. Hoffman, J. Jacobs, M. J. Kahana, L. Li, Z. Liao, J. J. Lin, A. Losonczy, R. Malach, M. A. van der Meer, K. McClain, B. L. McNaughton, Y. Norman, A. Navas-Olive, L. M. de la Prida, J. W. Rueckemann, J. J. Sakon, I. Skelin, I. Soltesz, B. P. Staresina, S. A. Weiss, M. A. Wilson, K. A. Zaghloul, M. Zugaro, G. Buzsáki, A consensus statement on detection of hippocampal sharp wave ripples and differentiation from other fast oscillations, Nature Communications 13 (1) (2022) 6000, number: 1 Publisher: Nature Publishing Group. doi:10.1038/s41467-022-33536-x.
URL https://www.nature.com/articles/s41467-022-33536-x

[40] K. Kay, M. Sosa, J. E. Chung, M. P. Karlsson, M. C. Larkin, L. M. Frank, A hippocampal network for spatial coding during immobility and sleep, Nature 531 (7593) (2016) 185–190. doi:10.1038/nature17144.

[41] L. McInnes, J. Healy, N. Saul, L. Großberger, UMAP: Uniform Manifold Approximation and Projection, Journal of Open Source Software 3 (29) (2018) 861. doi:10.21105/joss.00861.
URL https://joss.theoj.org/papers/10.21105/joss.00861

[42] P. J. Rousseeuw, Silhouettes: A graphical aid to the interpretation and validation of cluster analysis, Journal of Computational and Applied Mathematics 20 (1987) 53–65. doi:10.1016/0377-0427(87)90125-7.
URL https://www.sciencedirect.com/science/article/pii/0377042787901257

[43] P. Virtanen, R. Gommers, T. E. Oliphant, M. Haberland, T. Reddy, D. Cournapeau, E. Burovski, P. Peterson, W. Weckesser, J. Bright, S. J. van der Walt, M. Brett, J. Wilson, K. J. Millman, N. Mayorov, A. R. J. Nelson, E. Jones, R. Kern, E. Larson, C. J. Carey, Polat, Y. Feng, E. W. Moore, J. VanderPlas, D. Laxalde, J. Perktold, R. Cimrman, I. Henriksen, E. A. Quintero, C. R. Harris, A. M. Archibald, A. H. Ribeiro, F. Pedregosa, P. van Mulbregt, SciPy 1. 0 Contributors, SciPy 1.0: fundamental algorithms for scientific computing in Python, Nature Methods 17 (2020) 261–272, aDS Bibcode: 2020NatMe..17..261V. doi:10.1038/s41592-019-0686-2.
URL https://ui.adsabs.harvard.edu/abs/2020NatMe..17..261V

[44] G. Buzsáki, Two-stage model of memory trace formation: a role for "noisy" brain states, Neuroscience 31 (3) (1989) 551–570. doi:10.1016/0306-4522(89)90423-5.

[45] M. L. V. Quyen, A. Bragin, R. Staba, B. Crépon, C. L. Wilson, J. Engel, Cell Type-Specific Firing during Ripple Oscillations in the Hippocampal Formation of Humans, Journal of Neuroscience 28 (24) (2008) 6104–6110, publisher: Society for Neuroscience Section: Brief Communications.

doi:10.1523/JNEUROSCI.0437-08.2008.
URL https://www.jneurosci.org/content/28/24/6104

[46] S. Royer, B. V. Zemelman, A. Losonczy, J. Kim, F. Chance, J. C. Magee, G. Buzsáki, Control of timing, rate and bursts of hippocampal place cells by dendritic and somatic inhibition, Nature Neuroscience 15 (5) (2012) 769–775, number: 5 Publisher: Nature Publishing Group. doi:10.1038/nn.3077.
URL https://www.nature.com/articles/nn.3077

[47] N. Hájos, M. R. Karlócai, B. Németh, I. Ulbert, H. Monyer, G. Szabó, F. Erdélyi, T. F. Freund, A. I. Gulyás, Input-output features of anatomically identified CA3 neurons during hippocampal sharp wave/ripple oscillation in vitro, The Journal of Neuroscience: The Official Journal of the Society for Neuroscience 33 (28) (2013) 11677–11691. doi:10.1523/JNEUROSCI.5729-12.2013.

[48] E. W. Schomburg, C. A. Anastassiou, G. Buzsáki, C. Koch, The Spiking Component of Oscillatory Extracellular Potentials in the Rat Hippocampus, The Journal of Neuroscience 32 (34) (2012) 11798–11811. doi:10.1523/JNEUROSCI.0656-12.2012.
URL https://www.ncbi.nlm.nih.gov/pmc/articles/PMC3459239/

[49] X. Liu, S. Ramirez, P. T. Pang, C. B. Puryear, A. Govindarajan, K. Deisseroth, S. Tonegawa, Optogenetic stimulation of a hippocampal engram activates fear memory recall, Nature 484 (7394) (2012) 381–385, number: 7394 Publisher: Nature Publishing Group. doi:10.1038/nature11028.
URL https://www.nature.com/articles/nature11028

Contributors

Y.W. and T.Y. conceptualized the study; Y.W. performed the data analysis; Y.W. and T.Y. wrote the original draft; and all authors reviewed the final manuscript.

Acknowledgments

This research was funded by a grant from the Exploratory Research for Advanced Technology (JPMJER1801).

Declaration of Interests

The authors declare that they have no competing interests.

Data and code availability

The data is available on G-Node (https://doi.gin.g-node.org/10.12751/g-node.d76994/). The source code is available on GitHub (https://github.com/yanagisawa-lab/hippocampal-neural-fluctuation-during-a-WM-task-in-hum

Inclusion and Diversity Statement

We support inclusive, diverse, and equitable conduct of research.

Declaration of Generative AI in Scientific Writing

The authors employed ChatGPT, provided by OpenAI, for enhancing the manuscript's English language quality. After incorporating the suggested improvements, the authors meticulously revised the content. Ultimate responsibility for the final content of this publication rests entirely with the authors.

Tables

Subject ID	of sessions	AHL	AHR	PHL	PHR	ECL	ECR	AL	AR	SOZ
1	4	o	x	o	o	o	x	o	x	"AHR, LR"
2	7	o	o	o	o	o	o	o	o	"AHR, PHR"
3	3	o	o	o	o	o	o	o	x	"AHL, PHL"
4	2	o	o	o	o	o	o	o	o	"AHL, AHR, PHL, PHR"
5	3	o	x	x	o	x	x	o	x	DRR
6	6	o	o	o	o	o	o	o	o	"AHL, PHL, ECL, AL"
7	4	o	o	o	o	o	o	o	o	"AHR, PHR"
8	5	o	o	o	o	o	o	o	o	ECR
9	2	o	o	o	o	o	o	o	o	"ECR, AR"

Table 1 – Distribution of Electrodes within the Dataset Electrode Distribution within the Dataset

This figure represents denotes the electrode placements of electrodes and the seizure onset zones. Regions designated marked with were available included in the dataset, whereas while those marked imprinted with were not presentabsent. Abbreviations includeThe abbreviations used are as follows: AHL, left hippocampal head; AHR, right hippocampal head; PHL, left hippocampal body; PHR, right hippocampal body; ECL, left entorhinal cortex; ECR, right entorhinal cortex; AL, left amygdala; AR, right amygdala; and SOZ symbolizes represents the seizure onset zone.

Subject	AHL	AHR	PHL	PHR
1	0.60 ± 0.14	n.a.	n.a.	0.1 ± 0
2	0.21 ± 0.16	0.17 ± 0.21	0.18 ± 0.22	0.20 ± 0.15
3	0.40 ± 0.42	0.83 ± 0.12	n.a.	n.a.
4	0.10 ± 0.00	0.10 ± 0.00	0.90 ± 0.00	0.10 ± 0.14
5	n.a.	n.a.	n.a.	n.a.
6	0.63 ± 0.06	n.a.	n.a.	0.27 ± 0.06
7	0.10 ± 0.00	0.35 ± 0.35	0.37 ± 0.47	0.10 ± 0.00
8	0.13 ± 0.10	n.a.	0.28 ± 0.49	n.a.
9	n.a.	0.85 ± 0.07	0.15 ± 0.07	n.a.

Table 2 – ~~**Silhouette score of UMAP clustering for SWR^{+} candidates and SWR^{-} candidates**~~ **Silhouette score of UMAP clustering for SWR^{+} candidates and SWR^{-} candidates**

The silhouette scores (mean ±SD across sessions per subject) for UMAP clustering of

Subject ID	of sessions	of trials	ROI	of SWRs	SWR incidence [Hz]
#1	2	100	AHL	274	0.34
#3	2	97	AHR	325	0.42
#4	2	99	PHL	202	0.26
#6	2	100	AHL	297	0.37
#9	2	97	AHR	72	0.09
Total = 10	Total = 493	"Total = ~~1,170"~~ 1170	0.30 ± 0.13 (mean ± SD)		

Table 3 – Summary of Detected SWR Events

The table ~~collates~~ provides statistics of ~~putative~~ presumptive CA1 regions and SWR events. Only the ~~first~~ initial two sessions (sessions 1 and 2) from each subject were ~~analyzed~~ included in our analysis to ~~minimize~~ reduce sampling bias.

Figures

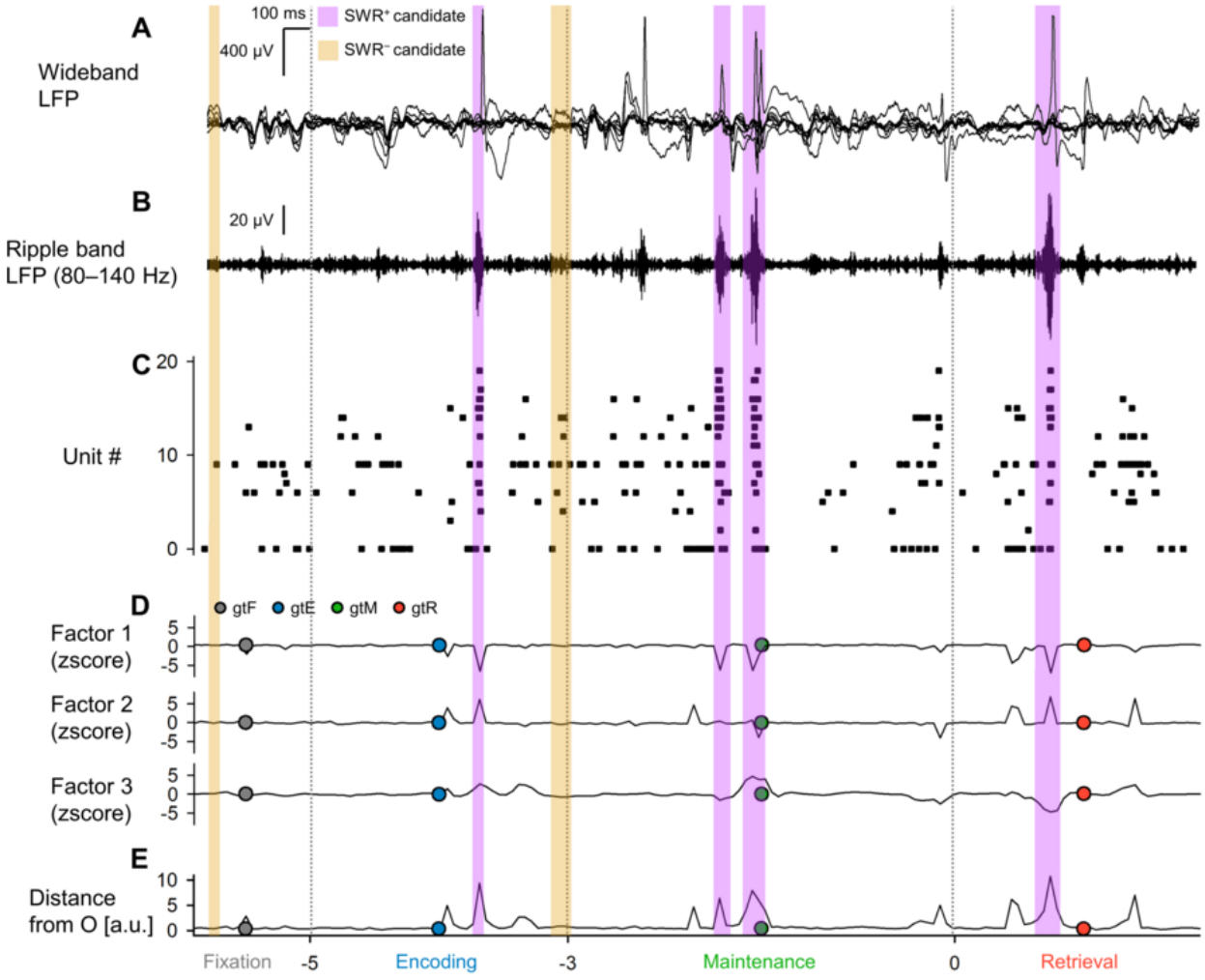

Figure 1 – Local Field Potentials (LFP), Multiunit Activity, and Neural Trajectories in the Hippocampus During a Modified Sternberg Task

A. ~~These traces show representative~~ Representative wideband LFP signals for intracranial EEG ~~(iEEG) signals recorded~~ recording from the left hippocampal head. The subject performed a modified Sternberg working memory task, which includes fixation (1 s, *gray*), encoding (2 s, *blue*), maintenance (3 s, *green*), and retrieval (2 s, *red*). ***B.*** ~~We then present the~~ The corresponding ripple band LFP traces. Note that *purple* and *yellow* rectangles indicating the timings for SWR$^+$ candidates and SWR$^-$ candidates (control events for SWR$^+$), respectively. ***C.*** The raster plot depicts multiunit spikes taken from the LFP traces, sorted using a spike algorithm [38]. ***D.*** ~~Subsequently, we illustrate the neural~~ Neural trajectories ~~, which are~~ calculated by GPFA[37] on spike counts per unit with 50-ms bins. Each phase's geometric median is marked by the dot circles. ***E.*** The ~~trajectory's~~ distance of neural trajectory from the origin *O*~~is portrayed, with *purple* and *yellow* rectangles indicating the timings for SWR$^+$ candidates and SWR$^-$ candidates (considered as controls for SWR$^+$), respectively~~.

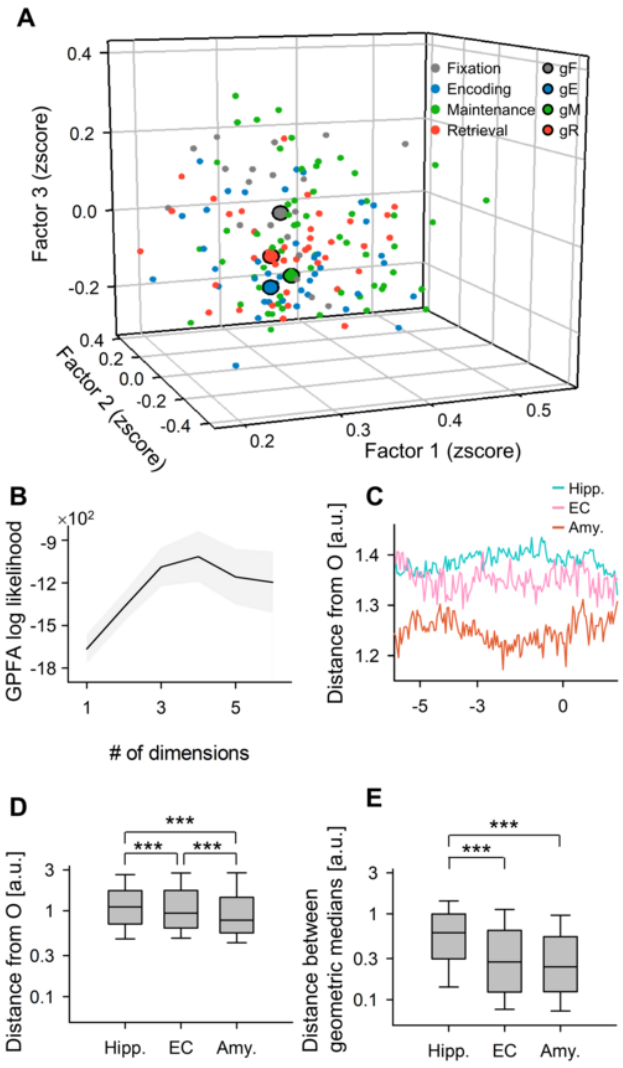

Figure 2 – State-Dependent Trajectories of Hippocampal Neurons

A. Neural trajectories as a point cloud within the initial three-dimensional factors derived from ~~the Gaussian Process Factor Analysis (~~GPFA ~~) are displayed~~[37]. The smaller dots correspond to coordinates of 50-ms neural trajectory bins, while the larger dots with *black* edges ~~signify~~ show the geometric medians for respective ~~stages~~ phases in the Sternberg working memory task: fixation ($\|g_F\|$, *gray*), encoding ($\|g_E\|$, *blue*), maintenance ($\|g_M\|$, *green*), and retrieval ($\|g_R\|$, *red*). ***B.*** The figure conveys the log-likelihood of the GPFA models versus the count of dimensions used to embed multiunit spikes found in the medial temporal lobe (MTL) territories. In specific, the elbow method pinpointed the optimal dimension to be three. ***C.*** This panel illustrates the distance of the neural trajectories from the origin (O) for the hippocampus (Hipp.), entorhinal cortex (EC), and amygdala (Amy.), against the time elapsed from the probe onset. ***D.*** The distance of the trajectory from O within MTL regions is displayed. The hippocampus shows the farthest distance, followed by the EC and the Amygdala. ***E.*** The box plot represents inter-phase trajectory distances within the MTL regions. ~~Abbreviations:~~

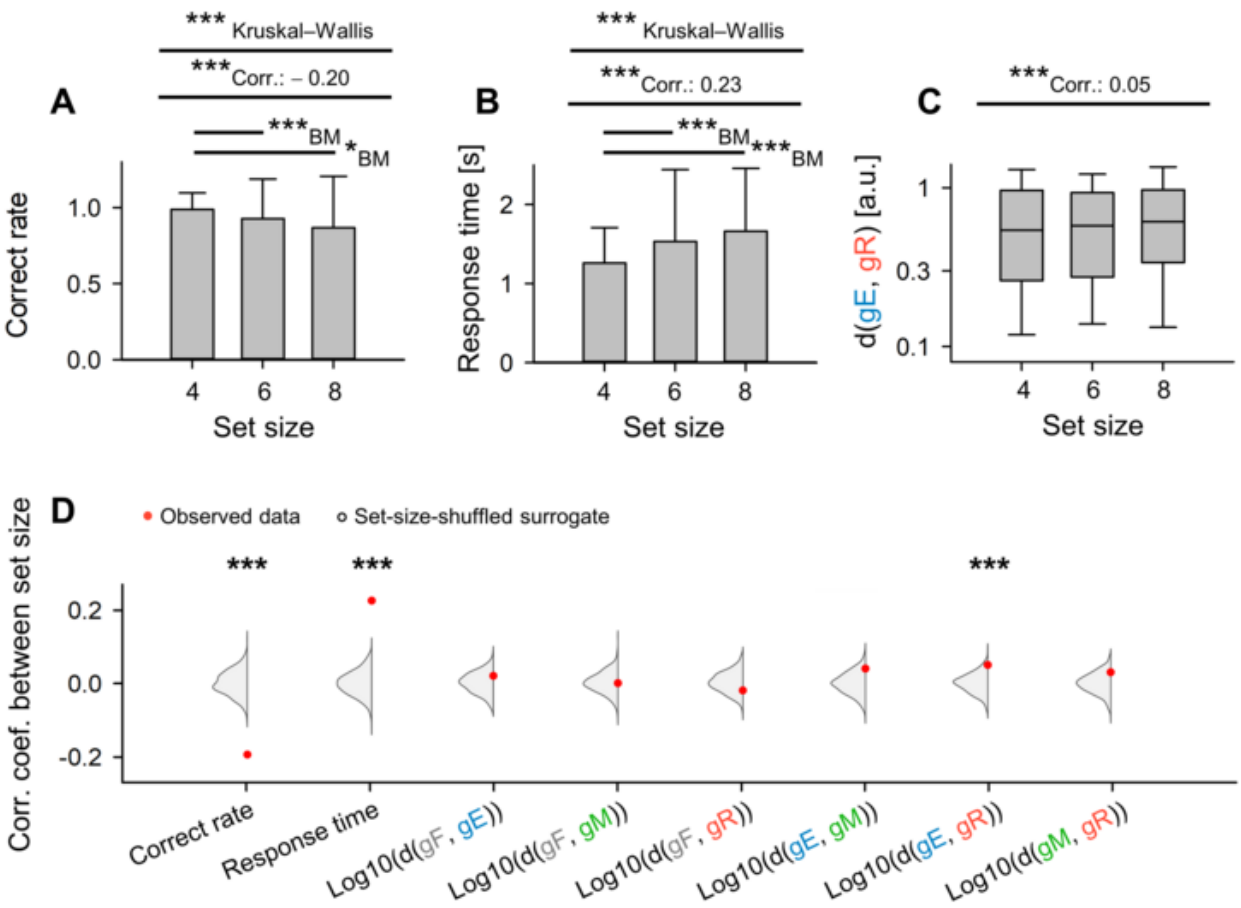

Figure 3 – Dependency of Trajectory Distance on Memory Load: Encoding and Retrieval States in Hippocampus

A. The relationship between set size (number of letters that need to be encoded) and correct rate in the working memory task (coefficient = −0.20, ***$p < 0.001$). ***B.*** The correlation between set size and response time (coefficient = 0.23, ***$p <$ 0.001). ***C.*** The impact of set size on the inter-phase distances between the encoding and retrieval phases ($\|g_E g_R\|$) (correlation coefficient = 0.05, ***$p < 0.001$). ***D.*** *Red* dots represent experimental observations of correlations between set size and the following parameters: correct rate, response time, $\log_{10}\|g_F g_E\|$, $\log_{10}\|g_F g_M\|$, $\log_{10}\|g_F g_R\|$, $\log_{10}\|g_E g_M\|$, $\log_{10}\|g_E g_R\|$, and $\log_{10}\|g_M g_R\|$. The *gray* kernel density ~~plot illustrates~~ plots illustrate the corresponding set-size-shuffled surrogate (n = 1,000) (***ps < 0.001).

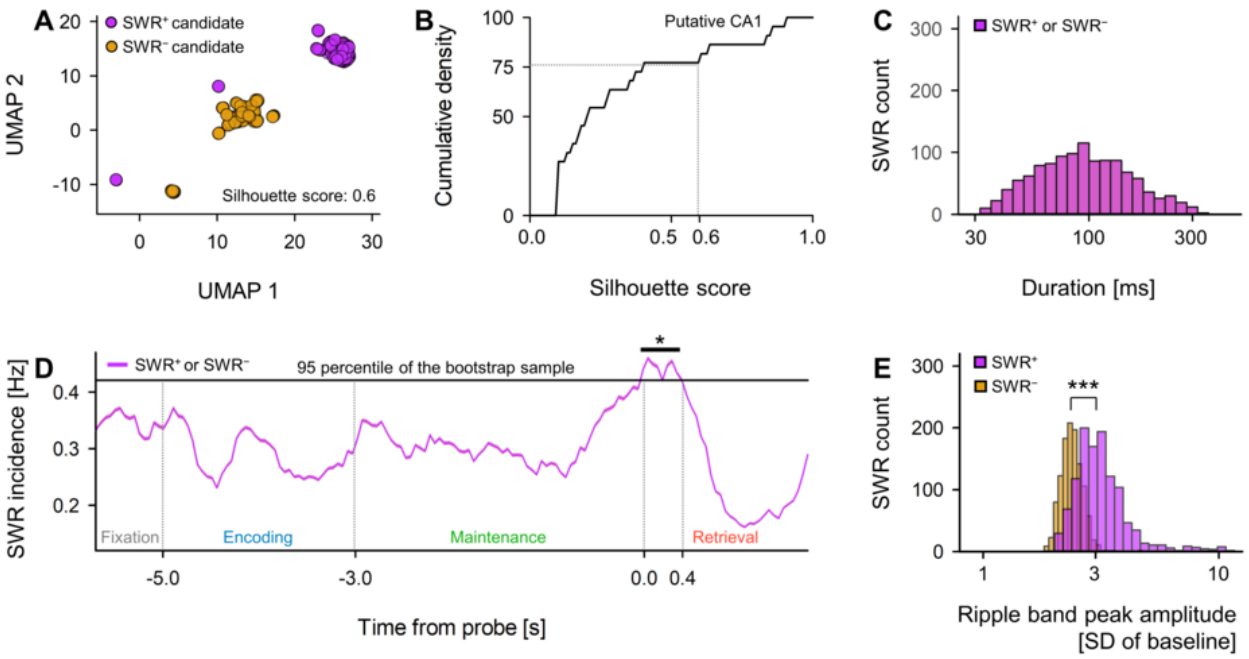

Figure 4 – Detection of SWRs in Presumptive CA1 Regions

A. Two-dimensional UMAP ~~(Uniform Manifold Approximation and Projection)~~ [41] projection of multiunit spikes during SWR$^+$ candidates (*purple*) and SWR$^-$ candidates (*yellow*). ***B.*** Cumulative density plot ~~shows~~ showing silhouette scores, indicative of UMAP clustering quality ~~, for hippocampal regions~~ (see Table 2~~for reference~~). Note that hippocampal regions with silhouette scores greater than 0.60 (equivalent to the 75th percentile) were ~~identified~~ defined as ~~possible~~ putative CA1 regions. SWR$^+$ and SWR$^-$ candidates recorded from these ~~speculative~~ putative CA1 regions were respectively classified as SWR$^+$ and SWR$^-$ (*n*s = 1,170). ***C.*** The identical distributions of durations are presented for SWR$^+$ (*purple*) and SWR$^-$ (*yellow*), owing to their definitions (93.0 [65.4] ms, median [IQR]). ***D.*** SWR incidence for both SWR$^+$ (*purple*) and SWR$^-$ (*yellow*) obtained relative to the probe's timing is illustrated as a mean ±95% confidence interval. However, as the intervals may not be visible due to their narrow ~~range~~ranges, note that a significant increase in SWR incidence was detected during the initial 400 ms of the retrieval phase (0.421 [Hz], $*p < 0.05$, bootstrap test). ***E.*** The distributions of ripple band peak amplitudes for SWR$^-$ (*yellow*; 2.37 [0.33] SD of baseline, median [IQR]) and SWR$^+$ (*purple*; 3.05 [0.85] SD of baseline, median [IQR]) are delineated ($***p < 0.001$, the Brunner–Munzel test).

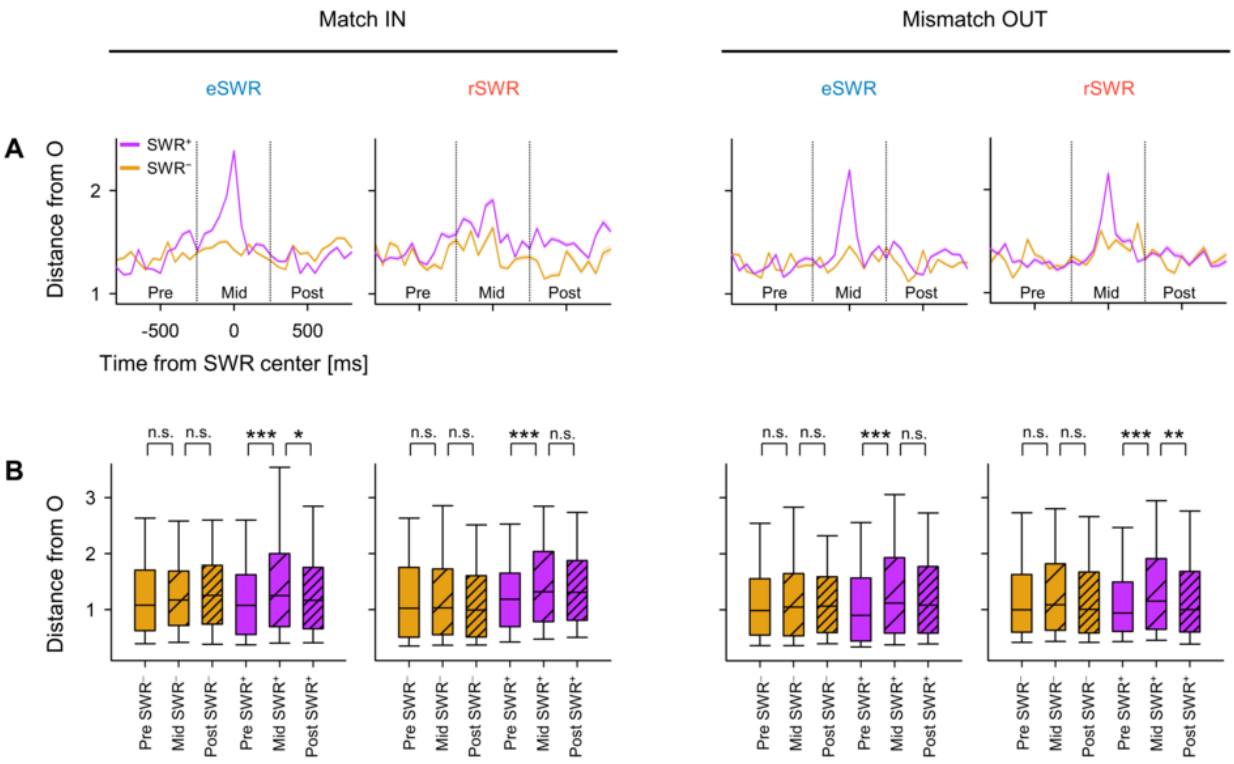

Figure 5 – Transient Alterations in Neural Trajectory During SWR Events

A. Displayed is the distance from origin (O) of the peri-sharp-wave-ripple trajectory (mean ±95% confidence interval). The intervals may not be apparent due to their ~~slender~~ narrow ranges. ***B.*** Shown is the distance from the origin (O) during pre-, mid-, and post-SWR periods (*$p < 0.05$, **$p < 0.01$, ***$p < 0.001$; ~~assessed using~~ the Brunner–Munzel test). Abbreviations: SWR, sharp-wave ripple events; eSWR, SWR during the encoding phase; rSWR, SWR while in the retrieval phase; SWR$^+$, positive SWR event; SWR$^-$, control events for SWR$^+$; pre-, mid-, or post-SWR denote the time intervals from −800 to −250 ms, from −250 to +250 ms, or from +250 to +800 ms, all relative to the center of the SWR.

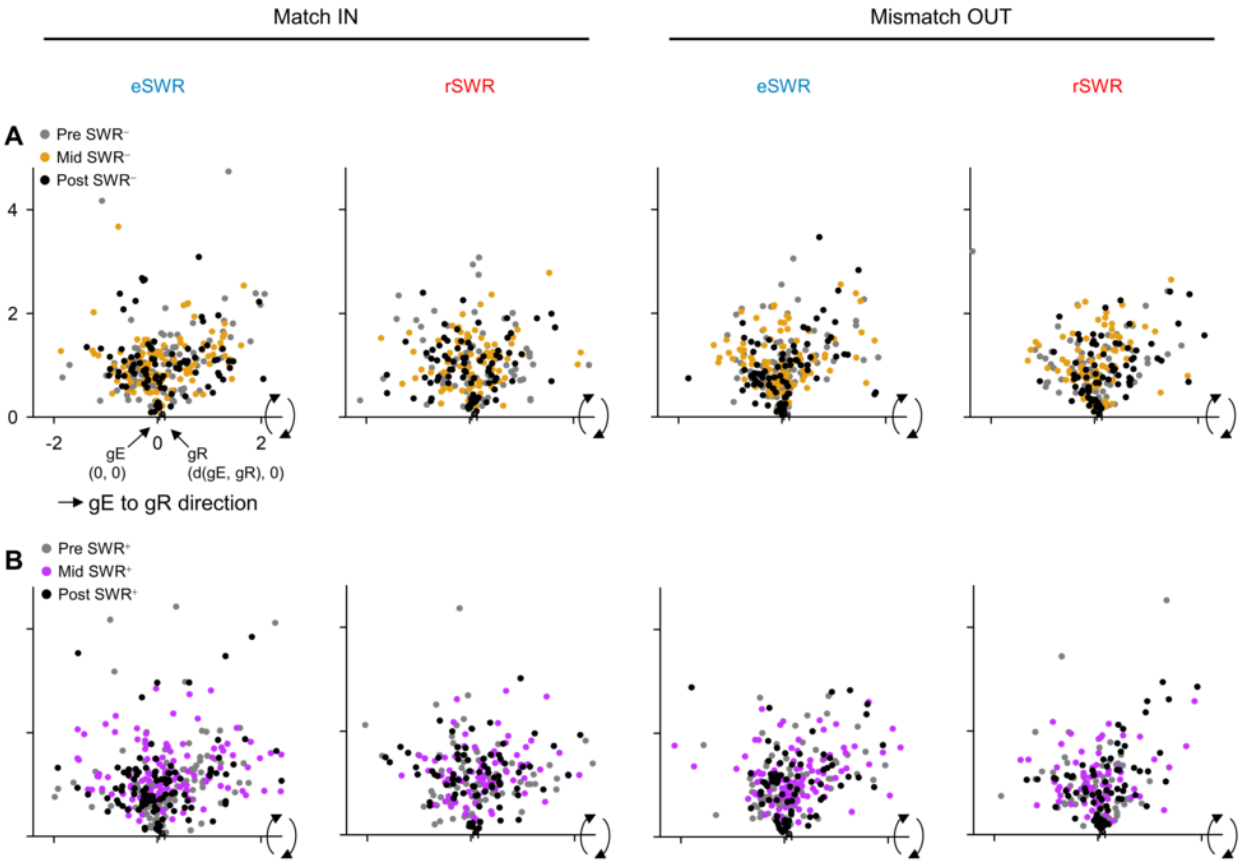

Figure 6 – Visualization of Neural Trajectories during SWR in Two-Dimensional Spaces

The panels display hippocampal neural trajectories during SWR as projected onto two-dimensional spaces. ***A.*** ~~Indicates hippocampal~~ Hippocampal neural trajectories as point clouds during pre-SWR$^-$ (*gray*), mid-SWR$^-$ (*yellow*), and post-SWR$^-$ (*black*). ***B.*** Represents the equivalents for SWR$^+$ as opposed to SWR$^-$. The ~~$\|g_E g_R\|$ varied among sessions. The~~ projection was applied in the following manner: First, a linear transformation positioned g_E at the origin O (0,0), and g_R at ($\|g_E g_R\|$, 0). The point cloud was then rotated around the $g_E g_R$ axis (equivalent to the x axis) for fitting into two-dimensional spaces. Therefore, within these two-dimensional spaces, both the distances from O and the angles ~~preserved the original makeup of~~ for the $g_E g_R$ axis ~~from~~ are preserved the original ~~three-dimensional~~ three dimensional spaces in GPFA. Abbreviations: SWR signifies sharp-wave ripple events; eSWR denotes SWR during the encoding phase; rSWR indicates SWR during the retrieval phase; SWR$^+$, marks an SWR event; SWR$^-$ refers to control events for SWR$^+$; pre-SWR, mid-SWR, or post-SWR, reference the time intervals from −800 to −250 ms, from −250 to +250 ms, or from +250 to +800 ms from the center of SWR.

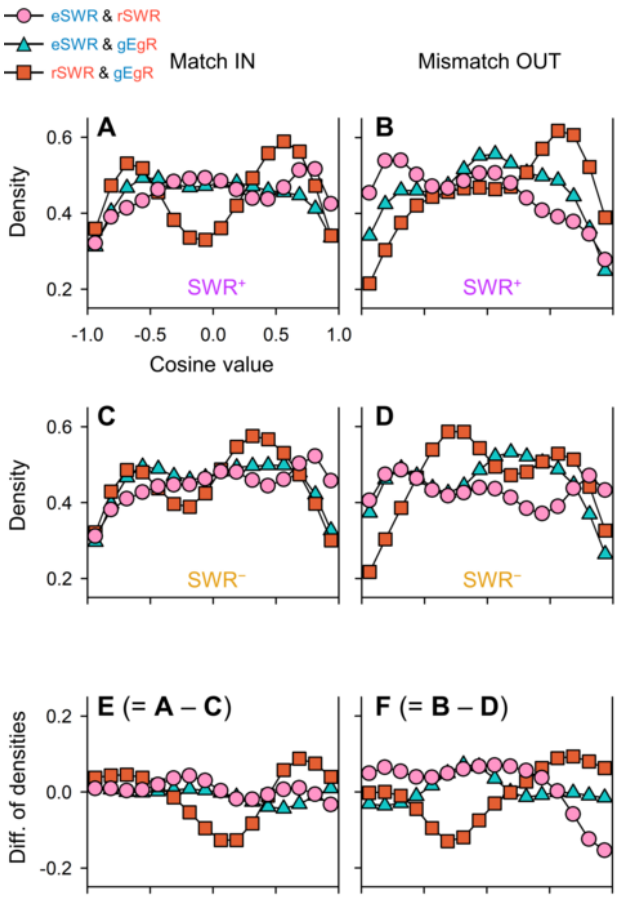

Figure 7 – Directions of Neural Trajectories during SWRs Based on Encoding and Retrieval States

A–B Kernel density estimation ~~(KDE)~~ distributions of $\overrightarrow{\text{eSWR}^+} \cdot \overrightarrow{\text{rSWR}^+}$ (*pink circles*), $\overrightarrow{\text{eSWR}^+} \cdot \overrightarrow{g_E g_R}$ (*blue triangles*), and $\overrightarrow{\text{rSWR}^+} \cdot \overrightarrow{g_E g_R}$ (*red rectangles*) in Match In (*A*) and Mismatch OUT tasks (*B*). ***C–D*** Present the corresponding distributions of SWR^- instead of those of SWR^+ in *A* and *B*. ***E–F*** Depict the differences in the distributions of SWR^+ and SWR^-, illuminating the SWR components ($E = C - A$ ~~;~~ & $F = D - B$). Note the biphasic distributions of $\overrightarrow{\text{rSWR}^-} \cdot \overrightarrow{g_E g_R}$, suggesting fluctuations between the encoding and retrieval states during the Sternberg task. Moreover, inverse directionality between $\overrightarrow{\text{eSWR}^+}$ and $\overrightarrow{\text{rSWR}^+}$ was observed (*pink circles*) ~~in the Mismatch OUT task, but~~ not in the Match IN task ~~***E–F***~~***E***~~.~~) but in Mismatch OUT task ***F***), Finally, shifts from the retrieval to encoding states ~~were evident~~ are acknowledged in the SWR components in both ~~the~~ Match IN and Mismatch OUT tasks (*red rectangles* in ~~*E* and *F*~~*E–F*).